

---

# Geophysics and Remote Sensing

Sverre Planke, Henrik Svensen, Reidun Myklebust,  
Stephen Bannister, Ben Manton, and Lars Lorenz

---

## Abstract

Igneous sheet intrusions such as sills, dikes, and laccoliths are abundant in volcanic basins. Mafic intrusions are characterized by high P-wave seismic velocities in the range from 5.0 to 7.0 km/s. Velocity aureoles with a thickness comparable to the sill intrusion are commonly identified on sonic log data above and below the intrusions. Sills as thin as 10 m may be detected by conventional seismic reflection data, whereas sills with a thickness above about 40 m are resolvable. Offset-dependent tuning of sill reflections is expected due to the high velocity of the intrusions. Deep sills are difficult to image by reflection methods but can be identified from wide-angle seismic data. Sill reflections are interpreted based on characteristic features such as their high amplitudes and saucer-shaped geometries. Sill complexes are further well-suited for 3D visualization techniques. Potential field and electromagnetic data may improve the reliability of the igneous intrusion interpretation; however such data have poor resolution if sills are buried below more than a few kilometers of sediments. Andesitic and felsic intrusions and laccoliths are less abundant than sills in volcanic basins, and few well-documented geophysical interpretation studies of such intrusions or dykes are published.

---

S. Planke (✉) · H. Svensen  
Centre for Earth Evolution and Dynamics (CEED),  
University of Oslo, Oslo, Norway  
e-mail: planke@vbpr.no

S. Planke  
Volcanic Basin Petroleum Research (VBPR),  
Oslo Science Park, Oslo, Norway

R. Myklebust  
TGS, Asker, Norway

S. Bannister  
GNS Science, Lower Hutt, New Zealand

B. Manton  
Cardiff University, Cardiff, UK

L. Lorenz  
EMGS, Oslo, Norway

---

## 1 Introduction (F1-3)

Igneous sheet intrusions are commonly present in sedimentary basins world-wide, and are associated with continental and volcanic rifted margin Large Igneous Provinces (LIPs). The intrusions are dominantly mafic in composition, however ultramafic, andesitic, and felsic LIPs are also identified (Bryan and Ernst 2008; Bryan and Ferrari 2013). The subvolcanic intrusions in sedimentary basins are dominantly tabular in shape, whereas laccoliths and plutons are less abundant. Smaller volume igneous intrusions are

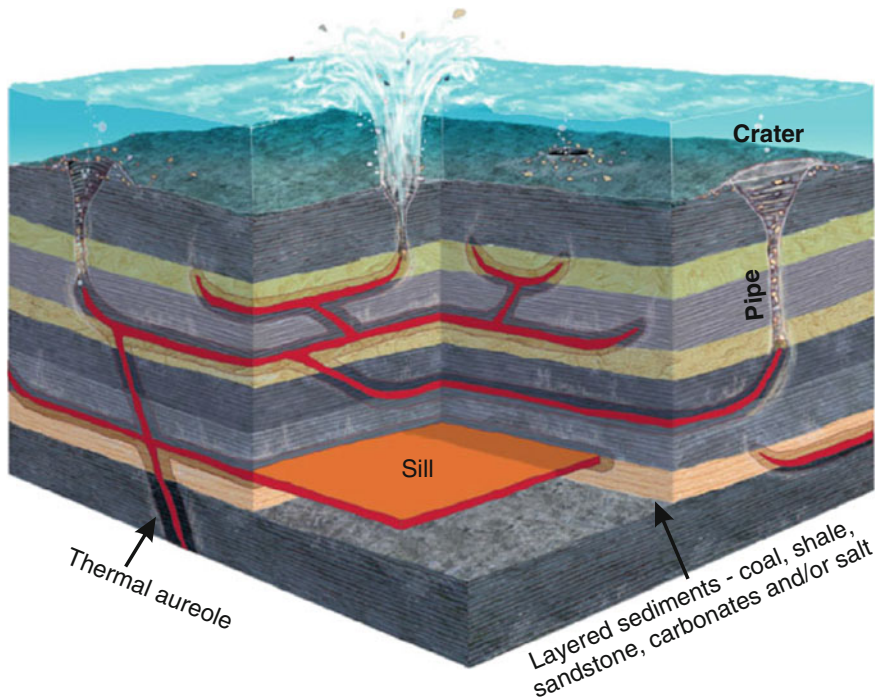


**Fig. 1** Sketch of a volcanic basin showing a sill complex (red), thermal aureoles and associated hydrothermal vent complexes. The vent complexes are typically located

above the tip of transgressive sills, and consist of a vertical pipe and a crater at the seabed

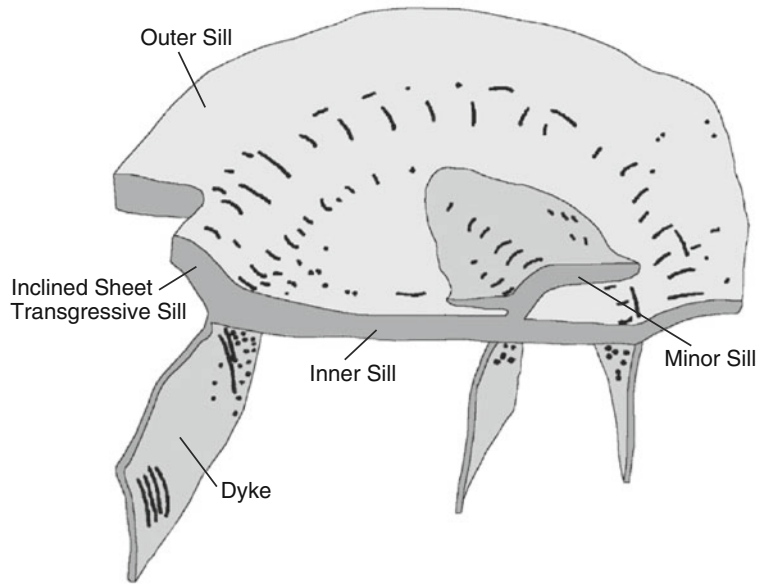
also present in sedimentary basins and sedimentary sequences above oceanic crust.

The emplacement of magma into sedimentary basins causes heating and deformation of the host rocks. Metamorphic reactions may lead to the formation of large volumes of greenhouse gases such as methane and carbon dioxide, or ozone-depleting gases such as chlorinated and brominated halocarbons if evaporite basins are intruded. It has been suggested that rapid release of such gases to the atmosphere may have triggered rapid global warming and mass-extinction events several times during Earth history (e.g., Svensen et al. 2004). The igneous intrusions also have an impact on the petroleum and mineral prospectivity of sedimentary basins. The sill complexes may represent long-lasting barriers to fluid flow, whereas fracture contact zones and hydrothermal vent complexes may lead to focused fluid flow. The permeable zones are good targets for water exploration drilling in dry

regions such as the Karoo of South Africa (Chevallier and Woodford 1999).

Volcanic basins are sedimentary basins with major components of intrusive and/or extrusive igneous rocks. Figure 1 shows a sketch of a subvolcanic complex in a typical volcanic basin. Deep seated sills are dominantly layer parallel, whereas saucer-shaped sills are more common in the shallow intervals. The sills may form interconnected complexes, whereas dykes are less common. Metamorphic aureoles develop around the cooling intrusions. The heating causes devolatilization reactions, leading to overpressure by the formation of gases such as methane, carbon dioxide, and/or boiling of water below the critical pressure. Hydrothermal vent complexes are formed if sufficiently large pressures are generated to fracture the overburden in low-permeability sequences. The vent complexes commonly originate from the upper terminations of transgressive sill segments, and consist of a

**Fig. 2** Morpho-structural diagram of a typical saucer-shaped dolerite sill of the Karoo Basin. Note that the feeder dykes are often difficult to identify in the field. Modified from Chevallier and Woodford (1999)



pipe connecting the aureole to a crater at the paleo-surface.

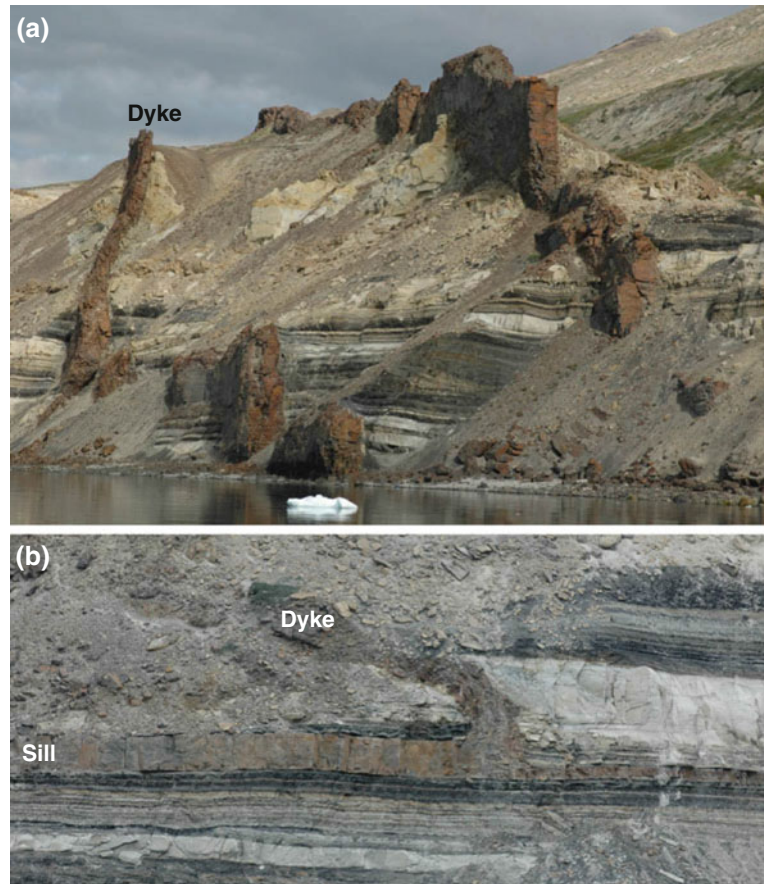
The sills commonly display a saucer-shaped geometry in layered sedimentary basins (Polteau et al. 2008). Field and borehole studies in the Karoo Basin reveal that the saucer-shaped sills consist of three main components: a sub-horizontal inner sill, inclined sheets (transgressive sills), and outer sills (Fig. 2). Minor sills and dykes are sometimes also present, but the feeding relationships of dykes and sills are often difficult to document. Figure 3 shows small-scale outcrops of near-vertical dykes and a rare occurrence of a sill-dyke connection in the Nuussuaq Basin, west-central Greenland.

Sub-horizontal sheet intrusions are well imaged on seismic reflection data as the sill-sediment contacts are high-impedance boundaries. Major sill complexes were identified on 2-D seismic data in the Northeast Atlantic in the 1980s and 1990s (e.g., Gibb and Kanaris-Sotiriou 1988; Skogseid and Eldholm 1989; Skogseid et al. 1992). During the past decade numerous detailed 3-D seismic studies of sill complexes have been published, in particular from the West of Shetland region (e.g., Bell and Butcher 2002; Trude 2004;

Hansen et al. 2004; Thomson 2004; Smallwood and Harding 2009). Saucer-shaped sill complexes are now identified in numerous sedimentary basins world-wide, including offshore West Africa (e.g., Rocchi et al. 2007) and Australia (Schofield and Totterdell 2008; Magee et al. 2013). In contrast, identification of dykes or intrusive bodies such as laccoliths, stocks and plutons is less common.

The aim of this contribution is to show how igneous intrusions are identified and interpreted on remote sensing geophysical data. The focus of the paper is on seismic imaging and interpretation of mafic sill complexes, as mafic intrusions are abundant in sedimentary basins and the seismic reflection method represents the most useful geophysical method currently available. However, potential field data (gravity, magnetic), wide-angle velocity data, electromagnetic data, and satellite imaging data are occasionally used to identify and interpret subvolcanic intrusions and will therefore also be briefly discussed. The examples are mainly from the Vøring Basin offshore mid-Norway, where extensive Paleogene breakup-related sill complexes intrude dominantly Cretaceous sequences.

**Fig. 3** Paleogene sills and dykes intruding sandstones, shales and coals of the deltaic Cretaceous Atane Formation at Atanikerluk on the Nuussuaq Peninsula, west-central Greenland. The dykes in **a** are about 3.5 m wide. The sill in **b** is about 1 m wide



## 2 Seismic Reflection Method

A high-quality 2-D seismic reflection profile across the northern Vøring Basin is shown in Fig. 4a. This profile reveals an extensive, dominantly layer-parallel sill complex that was intersected by exploration well 6607/5-2 on the Utgard High in 1991. The well drilled a 91 m thick Upper Sill (US) and terminated 50 m into a Lower Sill (LS). In addition, a 3 m thick sill was penetrated 370 m above the US. The Upper and Lower sills are accurately dated by the TIMS zircon U-Pb method at  $55.6 \pm 0.3$  and  $56.3 \pm 0.4$  Ma, respectively (Svensen et al. 2010). A detailed geochemical study of borehole cuttings shows that the dolerites were formed by fractional crystallization of melt in the lower

crust with minor assimilation of crustal melts, leaving a >320 m thick unit of ultramafic cumulates (Neumann et al. 2013).

The Upper Sill correlates with a high amplitude reflection, S1, in the Någrind Syncline, whereas the Lower Sill is less-well imaged in the Utgard High but can be correlated with S2 in the Någrind Syncline. Two deeper levels of sills, S3 and S4, are interpreted in the central part of the syncline. The imaging is not sufficiently good to determine if any deeper sills are present. Thin and small sills are also difficult to image, and the uppermost 3 m thick sill drilled in 6607/5-2 is too small to be imaged on available data. The vertical resolution limit of sills is discussed in Sect. 2.2. Note that no sills were intersected by the nearby well 6607/5-1, about 10 km to the southeast. No sill reflections are identified in this area.

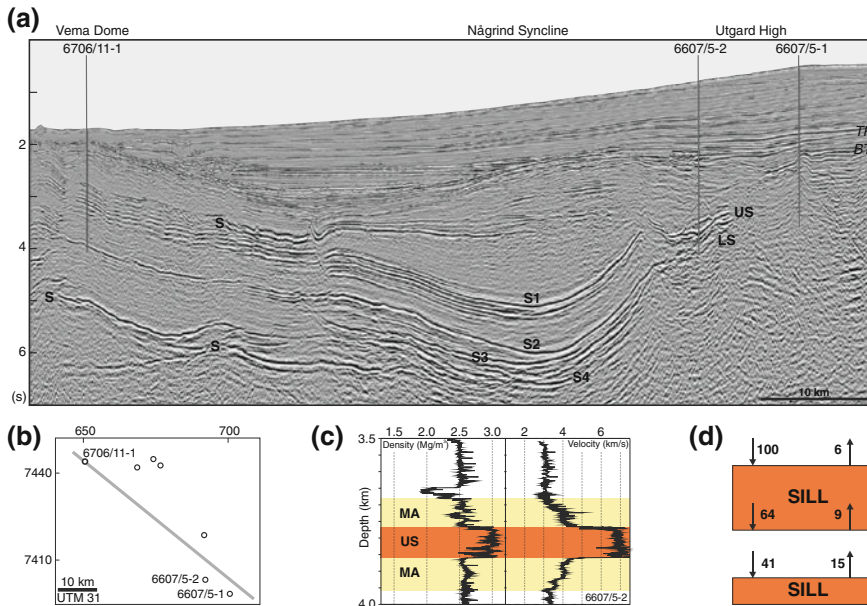


**Fig. 4** Seismic reflection profile across the north Vøring Basin in the Norwegian Sea. **a** 2D seismic reflection profile. **b** Location map; selected wells and seismic profile in **a** shown as circles and a grey line, respectively. **c** Wire line log data of the Upper Sill. **d** Normalized amplitude of transmitted and reflected normal incidence wave based on

Zoeppritz equations. Velocities of the host rock and sill are 3.0 and 5.5 km/s, respectively, whereas the corresponding densities are 2.5 and 2.9 Mg/m<sup>3</sup>. Modified from Planke et al. (2005). *S* sill; *US* upper sill; *LS* lower sill; *TP* top palaeocene; *BT* base tertiary

## 2.1 Petrophysics

The wire line logs from well 6607/5-2 document the characteristic petrophysical properties of dolerite intrusions. The sonic log shows a box like character, with a rapid increase of P-wave velocity at the top of the sill and a correspondingly rapid decrease at the base of the sill (Fig. 4c). The sill velocity is very high, about 7.0 km/s, and fairly constant throughout. A few zones of lower velocities correlate with increase in borehole size measured by the caliper log, and is likely related to hole washout, possibly related to fracturing of the dolerite.

The P-wave velocity of the intruded Upper Cretaceous sediments in the Utgard well is about 3.0 km/s. However, there is a distinct increase of P-wave velocity towards the sill both from the top and the bottom, reaching more than 4.0 km/s near the contact. The thickness of the interval with increased P-wave velocity is about 100 m both above and below the Upper Sill, defining a

high velocity contact metamorphic aureole around the intrusion (MA).

The entire suite of conventional log curves from the well is available from the Norwegian Petroleum Directorate ([www.npd.no](http://www.npd.no)). Other porosity-dependent logs (bulk density, neutron porosity, resistivity) reveal the same general trend as the sonic log. The dolerite density is as high as 3.0 Mg/m<sup>3</sup>, whereas the porosity is very low, typically <5%. The deep resistivity is very high (2,000 Ω-m; ca. 1–5 m depth of investigation), whereas the medium resistivity is somewhat lower (300–1,000 Ω-m). Shear wave velocity logs are not available, but Vp/Vs ratios of 1.8–2.0 are assumed based on downhole measurements of massive basalts in Ocean Drilling Program boreholes offshore southeast Greenland (Planke and Cambray 1998). The natural gamma ray log correlates well with the box-like velocity response, with a typical value of 30 GAPI in the dolerite. In the host rocks there is a well-defined intermediate resistivity aureole both above and below the

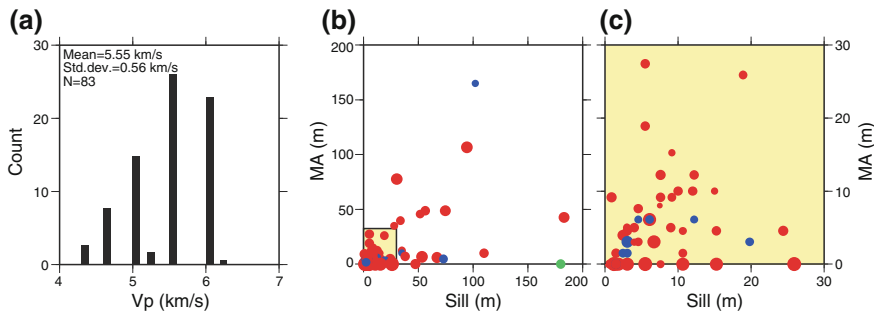


**Fig. 5** **a** Average P-wave wireline log velocities of 83 sills drilled West of Shetland. The average sill thickness is 35 m. **b**, **c** Sill versus metamorphic aureole (MA) thickness of the same sills. The sill and aureole thicknesses are interpreted from log data. *Red circles*

fine-grained clastic host rocks; *blue circles* limy fine-grained clastic host rocks. The symbol sizes are scaled according to the host rock velocity (mean of 3.55 km/s). Modified from Skogly (1998)

intrusion. No aureoles are identified on the gamma ray, density, and porosity logs.

Well log data from 83 sills drilled in the West of Shetland region reveal sonic velocities of 4.5–6.2 km/s, and a mean velocity of 5.55 km/s (Fig. 5a). These velocities are significantly lower than the Utgard sill velocities. The difference is possibly related to thickness, grain size, and compositional variations, with the Utgard sills being thicker and more iron-rich (Berndt et al. 2000). A plot of the sill versus the aureole thicknesses in the West of Shetland area displays a broad 1:1 correlation, however there is a large scatter of data and several intrusions with no detectable velocity aureoles.

Sill velocities may also be measured by wide-angle seismic experiments. A multi-layered sill complex, similar to the one in the Någrind Syncline, is found in the Hel Graben, about 50 km to the northwest. Berndt et al. (2000) modelled ocean bottom seismometer data across the Hel Graben, and obtained P-wave velocities of 7.4 km/s at ca. 5 km depth (Fig. 6), which is even higher than the 7.0 km/s sonic velocity of the Upper Sill of the Utgard well.

In summary, mafic sills represent high-velocity and high-density sheets in sedimentary basins. Seismically, they can be viewed as homogenous, isotropic layers. The intrusions are commonly associated with a velocity aureole of similar thickness to that of the sills, as confirmed by both mineralogical and thermal modelling (Aarnes et al. 2010). A caveat is that shallow sills and

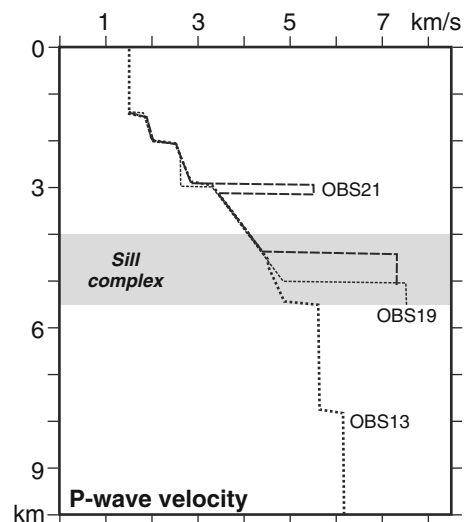


**Fig. 6** Seismic wide-angle velocity-depth profiles in the Hel Graben, about 50 km NW of the Vema Dome (Fig. 4). A layered sill complex intruded into Cretaceous sediments is associated with high P-wave velocities. *OBS* ocean bottom seismometer. Modified from Berndt et al. (2000)

invasive flows emplaced into unconsolidated sediments may have significantly lower velocities due to intense fracturing or the development of peperitic layers.

## 2.2 Seismic Imaging

High velocity tabular sill intrusions emplaced in low velocity host rocks represent easy targets for seismic imaging. Sub-sill imaging is, however,

more difficult, partly due to transmission loss across high-impedance contrast boundaries. This is clearly illustrated in Fig. 4a where the Upper Sill is much better imaged than the Lower Sill even though the sill-sediment impedance contrasts and the sill thicknesses are similar. The sketch in Fig. 4d shows the sub-sill decrease of reflection amplitude of a normal incidence plane-wave with a relative amplitude of 100. Based on Zoeppritz equations, the amplitude of the reflected wave from the top of the upper sill is six times greater than the amplitude of the reflected wave from the top of the lower sill. The figure shows that the relative amplitude of the wave reflected from the top of the lower sill is only 6 % of the amplitude of the incoming wave at the top of the upper sills.

Other factors influencing the seismic imaging are related to the geometry of the sills (e.g., thickness, areal extent, and dip). Additionally, the seismic acquisition parameters, such as the source pulse and streamer length, as well as seismic processing have an important impact on the imaging.

The seismic detection and resolution limits of sills depend on the signal/noise ratio and bandwidth of the data. In simple terms, detection is the ability to identify a sill, whereas resolution is the ability to determine the thickness of the intrusion. The vertical detection limit is perhaps as low as 1/30 of the dominant wavelength, or ca. 6 m for a 30 Hz wavelet and a sill velocity of 5.5 km/s. The horizontal detection limit is somewhat more difficult to assess. Pant and Greenhalgh (1989) used physical 2D seismic modelling to determine that targets as small as 1/30 of a wavelength are detectable, but the amplitude, polarity and frequency of the event is modified if the reflecting layer is less than one wavelength. The nature of the reflection is dependent on a volume integration of the properties of the media above and below the sill interface. The lateral extent of the integration volume corresponds to the first Fresnel zone at the sill-sediment interface (approximately 400–700 m radius for a 30 Hz reflection at 2–6 s depth and an average velocity of 3 km/s) (Favretto-Cristin et al. 2009). 3D migration is very

important for improved horizontal resolution, essentially for collapsing the Fresnel zone to a much smaller area.

The vertical seismic resolution of a thin bed is often determined by the classic quarter wavelength criterion. Thus, the vertical resolution of a sill with a velocity of 5.5 km/s is 46 and 69 m for a 30 and 20 Hz Ricker wavelet, respectively. However, thinner layers may be resolved down to 1/16 of a wavelength using spectral inversion methods (Purvey and Castagna 2008; Zhang and Castagna 2011). For real data, it is often the signal/noise ratio and the wavelet spectrum that determine the obtainable resolution limit.

Sill tuning and resolution aspects are explored using the classic wedge model of Widess (1973) and a 20 Hz zero-phase Ricker wavelet (Fig. 7). Note strong interference and tuning effects for sill thicknesses up to 120 m with destructive interference of <20 m thick sills and a maximum constructive interference for ca. 50 m thick sills.

Sills in volcanic basins are thin, high-velocity layers which lead to source-receiver offset dependent tuning of reflected waves. The tuning effects can be explored by full elastic wave-equation modelling of simplified Earth models and typical seismic acquisition parameters (Fig. 8). A 100 m thick sill is clearly resolved at short offsets for a 30 Hz Ricker wavelet. However, strong tuning effects are observed at offsets >2 km, and only one reflection is visible beyond 3 km offset. There is a clear amplitude-versus-offset (AVO) increase, with a peak near the critical offset. The tuning effects are similar for the sill and the sill+aureole models (Fig. 8c, d), however the maximum amplitude and the critical offset are slightly different with a lower near-offset amplitude and a greater critical distance of the sill +aureole model. Similar wave-equation modelling of 15–50 m thick sills show only one reflection at all offsets, and a clear AVO decrease.

Kinematic ray-tracing can be used to show how the distance between the top sill and base sill travel-time curves is reduced towards the critical point (Fig. 9). The decreasing separation between the two travel-time curves makes it more difficult to distinguish individual reflections with increasing offset and leads to offset-depending tuning.

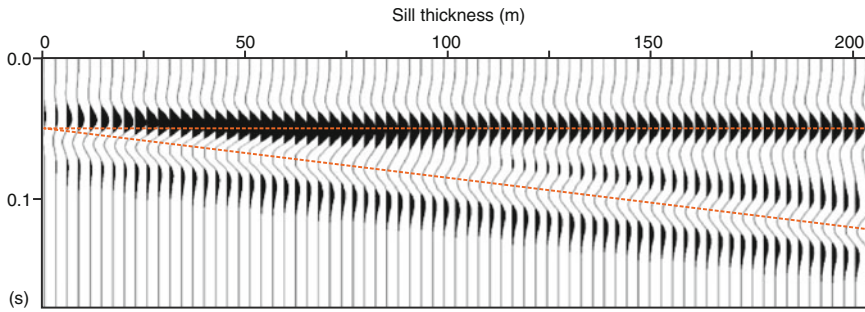


**Fig. 7** Plot of 1-D synthetic seismograms for sills with systematically increasing thicknesses from 0 to 205 m. The top and bottom sill contacts are shown by dashed orange lines. The section corresponds to perfectly

migrated reflection data. Calculations were done using a 20 Hz zero-phase Ricker wavelet and no transmission losses. Velocities of the host rock and sill are as in Fig. 4d

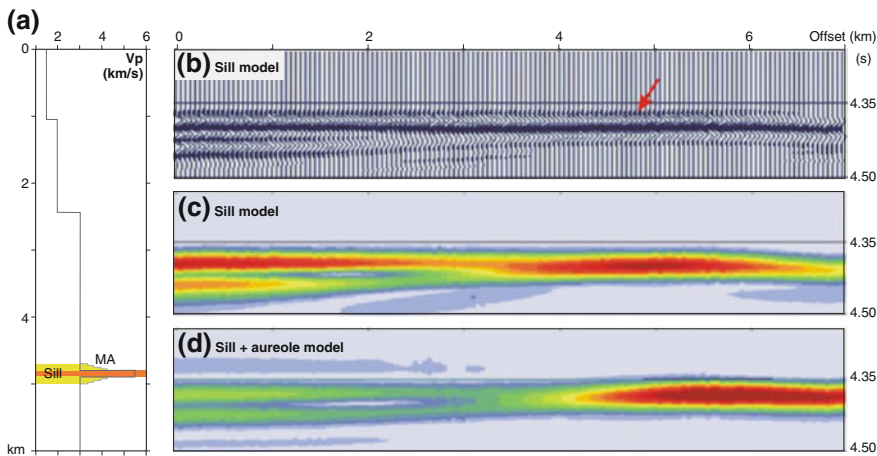


**Fig. 8** Synthetic wave-equation seismograms for a simplified 1-D Earth model showing strong source-receiver offset dependent tuning for a 100 m thick sill using a 30 Hz Ricker source wavelet. **a** P-wave velocity ( $V_p$ ) models of a 100 m thick sill with and without a metamorphic aureole (MA). Sediment layers  $\rho = 2.2 \text{ Mg/m}^3$ ,  $Q_p = Q_s = 250$ ;  $V_p/V_s = 1.8$  in upper sediment layer, 1.75 otherwise. Sill

intrusion  $\rho = 2.9 \text{ Mg/m}^3$ ,  $Q_p = Q_s = 1,000$ ,  $V_p/V_s = 1.9$ . **b** Synthetic seismograms of the sill model. Red arrow critical offset (4.8 km). The data are plotted after applying a static time-shift operator to align the sill reflections (i.e. no moveout stretching). **c, d** Instantaneous amplitude response of the sill model and sill + aureole model, respectively (red is high, blue is low; y-axis in seconds)

The wide-angle data from the Hel Graben (Fig. 6; Berndt et al. 2000) documents that sufficient seismic energy to be detected is transmitted through a sill-sediment complex with a wave velocity representing the high-velocity end-member ( $>7 \text{ km/s}$ ). The measured high velocity of the layered sill-sediment complex suggests that lower-crustal high velocity bodies imaged by wide-angle seismic data may not represent massive underplated material, but rather a complex of lower crustal intrusions mixed with sedimentary rocks (White et al. 2008).

### 2.3 Seismic Interpretation

The determination of lithology from seismic reflection data is challenging, in particular in frontier volcanic basins with limited well control. Igneous intrusions are, however, good imaging targets and have some deterministic features that make it possible to interpret them with high confidence in many basins. However, it is important to have consistent and reliable criteria to interpret intrusions and to avoid misinterpretation of similarly imaged geological features



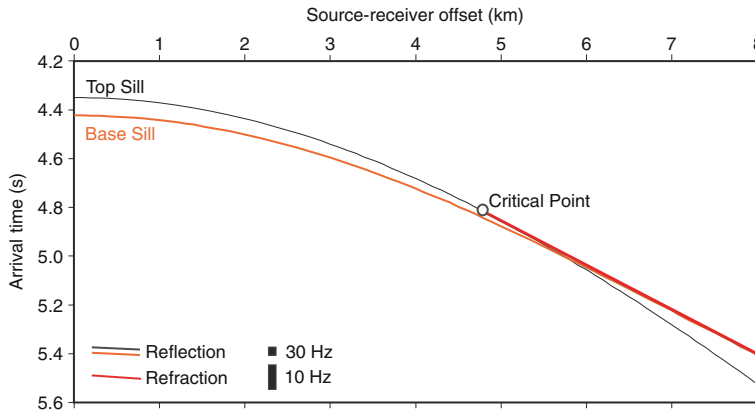


**Fig. 9** Kinematic ray-tracing of a four-layer Earth model (see Fig. 8a) with a 200 m thick sill. Note that the time-difference between the reflection curves from the upper

and lower surfaces decreases with offset. The critical offset for the top sill reflection is 4.8 km. Vertical length of 10 and 30 Hz wavelets shown

such as high-velocity carbonate layers, sediment intrusions, or gas-charged sandstones. Thin or small intrusions, dykes and other steeply dipping sheet intrusions, and intrusions below the uppermost igneous unit are also difficult to identify in many basin provinces.

A combination of methods is commonly used for interpretation of sill complexes in volcanic basins (Planke et al. 2005):

- horizon and attribute mapping,
- interpretation of sill reflections,
- 3D voxel visualization,
- seismic facies analyses, and
- integration with well, geological and other geophysical data.

The seismic interpretation is normally done in a workstation environment using software such as the Kingdom Suite ([www.ihs.com](http://www.ihs.com)) and Petrel ([www.software.slb.com](http://www.software.slb.com)). These software packages are well-suited for conventional mapping of time horizons and reflection attributes. Such data form an important stratigraphic framework for subsequent mapping of igneous intrusive units and associated hydrothermal vent complexes and lava flows.

Sill reflections are characterized by four distinct features:

- high positive reflection amplitudes,
- abrupt reflection terminations,
- saucer shape, and/or

- cross-cutting of layered sedimentary sequences (“transgressive sheets”).

The most diagnostic features are the high amplitude and the saucer-shape or transgressive nature of the sill reflections. 3D seismic data or grids of 2D seismic data are important to increase the confidence of the interpretation. An improved reliability can also be obtained by borehole calibration (e.g., Fig. 4), integration with other geophysical data (Sect. 3), and the identification of related igneous features in the basin.

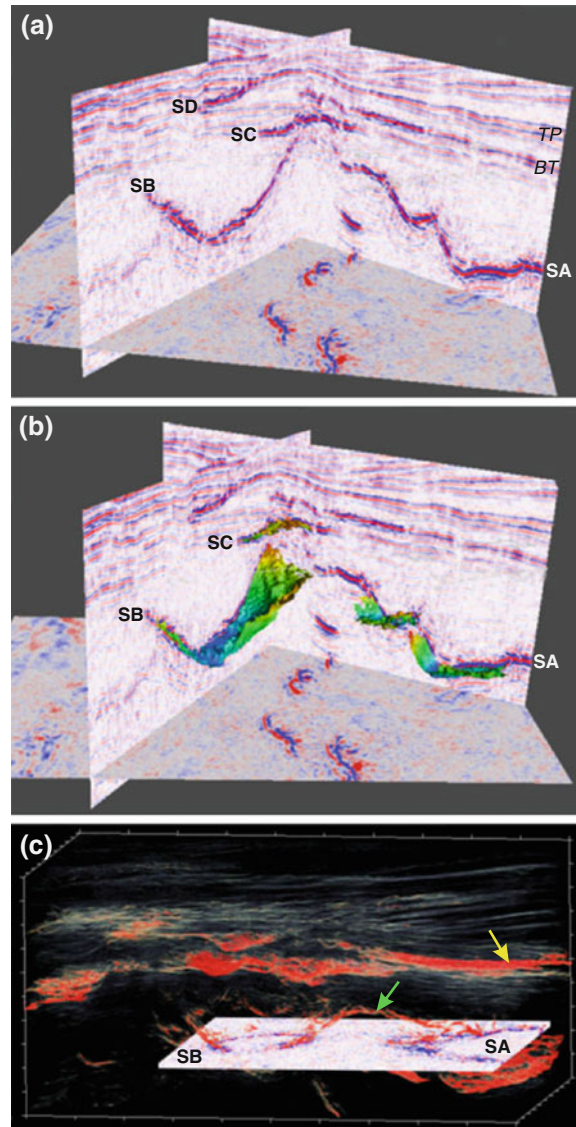
Sill complexes consist of splitting and merging sheets, and conventional horizon picking is therefore complicated. Normally, numerous horizons must be generated representing individual sill segments. In contrast, sill reflections are well suited for 3D visualization methods because of their high amplitudes and complicated shapes. Proper scaling of the data is obviously important, and true amplitude data or scaling using a long time window is useful for 3D visualization of sills.

Figure 10 shows the 3D interpretation of the Gleipne Sill Complex in the Outer Vøring Basin. Two saucer-shaped, positive high-amplitude reflections with abrupt terminations, SA and SB, are well-defined on seismic cross-sections and time slices (Fig. 10a). Two sub-horizontal high-amplitude events, SC and SD, are identified above the saucers. Both events are locally cross-cutting the uppermost Cretaceous and Palaeocene

**Fig. 10** 3-D visualization and interpretation of the Gleipne Sill Complex, outer Vøring Basin.

**a** Seismic profiles showing two well-defined saucer-shaped sills (*SA* and *SB*) and shallow sub-horizontal sills (*SC* and *SD*). The saucer-shaped sill *SB* is approximately  $3 \times 4$  km wide and 0.5 km high.

**b** Horizon interpretation of three sills. **c** Semi-transparent voxel rendering of reflection amplitudes. High amplitudes are shown in red. Green arrow possible link between *SA* and *SB*. Yellow arrow shallow sills



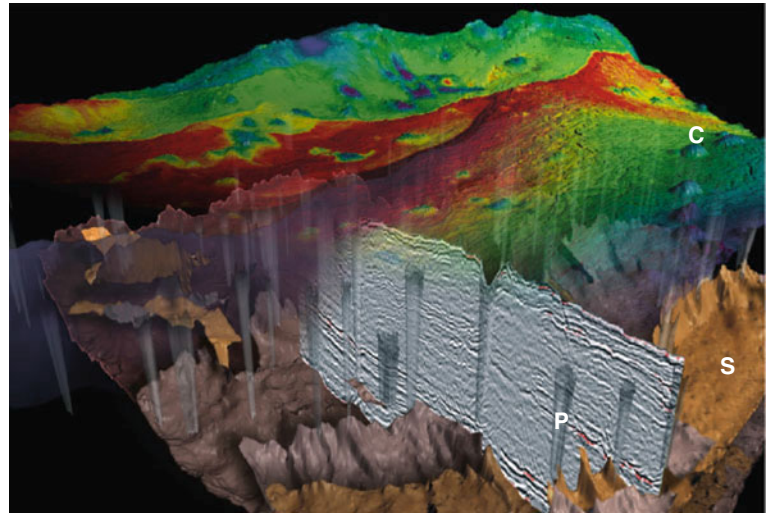
sequences below the Top Palaeocene (TP) paleosurface. These events are also interpreted as sills. A few discontinuous, high-amplitude layer-parallel events are also present in the Palaeocene sequence. No clear cross-cutting relationships are identified, and these events are therefore possibly sedimentary reflections.

The result of automatic horizon mapping of the two elliptical saucers, *SA* and *SB*, and the *SC* event, is shown in Fig. 10b. Semi-transparency amplitude voxel rendering reveal the saucer shape of *SA* and *SB* (Fig. 10c). These two saucers are

locally connected with an outer sill (green arrow). A visualization of the Stetind Sill Complex in the central Vøring Basin is shown in Fig. 11. Individual sills are picked and plotted as horizons. The sills are shown together with numerous vertical pipe structures terminating at kilometre-sized craters on the paleosurface. Mound structures are commonly present above the craters, both as domes near the Top Palaeocene horizon and in the overlying Eocene sequences.

Detailed sill interpretation, attribute analyses, and volume rendering techniques have

**Fig. 11** 3-D visualization of the Stetind Sill Complex in the central Vøring Basin. The interpreted sills (*S*) are associated hydrothermal vent complexes (*P* pipe; *C* crater/mound), and rms amplitudes of an Eocene time horizon. Visualization of Audun Groth, Statoil

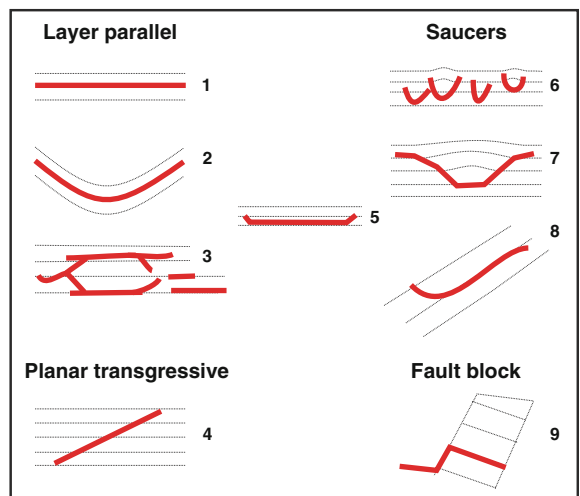


particularly been applied to 3D seismic data in the Northeast Atlantic to gain a better understanding of sill geometries and emplacement processes. Flow morphologies, magma tubes, and feeding systems have been mapped in detail (e.g., Trude 2004; Thomson 2004, 2007; Hansen et al. 2004; Cartwright and Hansen 2006; Hansen and Cartwright 2006a; Thomson and Schofield 2008; Smallwood and Harding 2009; Miles and Cartwright 2010; Schofield et al. 2012; Holford et al. 2012). The data document that sill complexes may form inter-connected plumbing systems with outward flow of magma in tubes and lobes. The sill emplacement leads to doming and deformation of sediments above saucer-shaped sills, forming

so-called forced-folds (Trude et al. 2003; Hansen and Cartwright 2006b). The Tulipan well in the Outer Møre Basin offshore mid-Norway made a small gas discovery in such a dome above a saucer-shaped sill (Polteau et al. 2008).

Sill reflections display a range of characteristic geometries that can be classified and mapped as facies units (Fig. 12; Planke et al. 2005). Saucer-shaped sills are formed when magma is injected into layered sedimentary basins due to uplift and elastic deformation of the overburden sediments (Polteau et al. 2008). The size of the saucer is a function of the emplacement depth, with small saucers or cone sheets formed at shallow depths whereas large saucers with minor

**Fig. 12** Sketch showing the geometries of sill facies units 1–9 in the Vøring Basin. Modified from Planke et al. (2005)



transgressive sheets are found at larger depths. Magma may also exploit weak sediment layers (e.g., shales) and fractures (e.g., faults) forming layer-parallel tabular sheets (Magee et al. 2013). Sub-horizontal invasive or hybrid flows and associated peperites are formed when magma intrudes unconsolidated sediments at very shallow emplacement depths (e.g., the yellow arrow shows high-amplitude shallow sills in Fig. 10c and Miles and Cartwright 2010).

Dykes and laccoliths are rarely identified in seismic data, even in high-quality 3D cubes. Dykes are frequently thin and steeply dipping (Fig. 3a) and are therefore difficult to image by the seismic reflection method. However, dyke swarms would be easily visible as linear amplitude anomalies on 3D time and horizon maps if they were abundant in the imaged areas. Laccoliths are mainly formed by low-volume injection of andesitic and felsic melt batches. Up to 500 m thick laccoliths are present in the Neuquén Basin, Argentina (Rodríguez Monreal et al. 2009). The laccoliths form an integrated part of the petroleum system in this basin, both by influencing the maturation of intruded immature source rocks and by forming fractured hydrocarbon reservoirs. Unfortunately, few seismic profiles are published from this region.

### 3 Other Geophysical Methods

The confidence of interpreted sill reflections can be increased through integration with other geophysical methods such as gravity, magnetic, wide-angle velocity and electromagnetic methods, and geological data. However, the resolution and detection limit of these data types are often insufficient to identify sheet intrusions in volcanic basins.

#### 3.1 Integrated Seismic, Gravity, Magnetic Interpretation

Mafic igneous intrusions are characterized by high magnetic susceptibilities and densities. However, sheet intrusions are normally quite thin, and give rise to small potential field

anomalies, particularly when the sheets are deeply buried in sedimentary basins. Anomalies are typically associated with rapid thickness variations or are edge effects. However, it is possible to image steeply dipping intrusions, such as dykes, or thick laccolith intrusions with high-resolution magnetic data.

Integrated seismic, gravity, and magnetic interpretation is done in a seismic workstation environment. High-pass filtered potential field data are scaled to two-way travel time, and imported as grids. This approach allows for plotting of the data as maps and curves on the seismic reflection data.

A seismic profile and 50-km high-pass filtered Bouguer gravity and magnetic anomaly maps are shown in Fig. 13. The profile is located in the Gjallar Ridge region in the outer Vøring Basin. Strong northeast trending magnetic anomalies, M1 and M2, are associated with the kilometre high Vøring Escarpment where subaerially emplaced basalt thins rapidly (Fig. 13a, b). The gravity anomaly displays a major sub-rounded positive anomaly associated with the Gjallar Ridge (Fig. 13c). Gravity modelling suggests that this anomaly is related to a deep density increase across the T-Reflection (Planke and Myklebust 1999; Gernigon et al. 2003). There is no good correlation between the gravity and magnetic anomaly, suggesting the body is non-magnetic. The interpretation of this high-density body is controversial, and several different models have been proposed including serpentinized mantle, a lower-crustal sill complex, a massive gabbroic magmatic underplate, and retrograde high-grade metamorphic rocks (Gernigon et al. 2004).

The seismic reflection data reveal several transgressive planar sheet intrusions climbing towards the Gjallar Ridge from the south and east. A deep sill intrusion is also imaged just northwest of the ridge. A minor magnetic anomaly, M3, is associated with the western edge of the sills in the Vigrid Syncline. The northeast trending anomaly extends along the eastern flank of the Gjallar Ridge for >10 km (Fig. 13b). Magnetic modelling suggests that the transgressive sills may be the cause of the M3 anomaly. Note that no gravity anomaly is associated with the sill terminations.

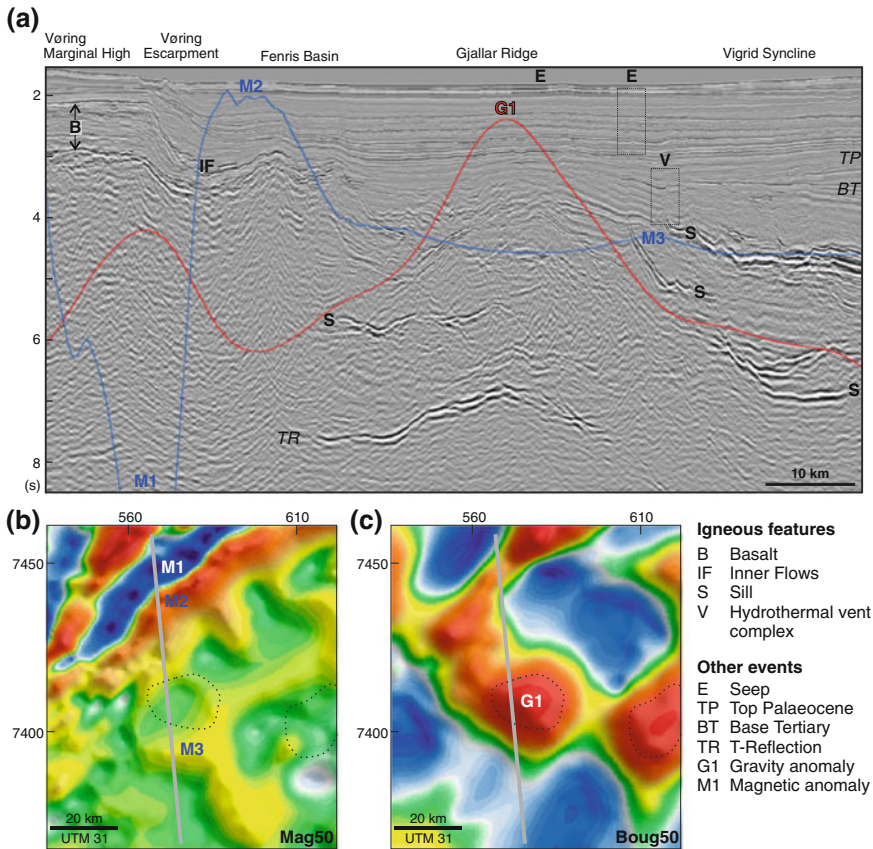


**Fig. 13** Integrated seismic-gravity-magnetic interpretation of the Gjallar Ridge, outer Vøring Basin. **a** Seismic profile extending from the Vøring Marginal High into the Vigrid Syncline. Gridded high-pass filtered gravity and magnetic data are converted to pseudo-time and displayed

as red and blue curves, respectively. **b** 50-km high-pass filtered aeromagnetic data. *Dashed lines* correspond to gravity anomalies. **c** 50-km high-pass filtered marine Bouguer gravity data

### 3.2 Wide-Angle Seismic and Electromagnetic Data

High-velocity and high-resistivity sill complexes can be imaged by wide-angle seismic profiling and electromagnetic data. However, the intrusions are commonly too thin to be detected by these methods, especially when they are deeply buried in sedimentary basins. A high-velocity sill complex is identified by wide-angle data in the northern Vøring Basin (Fig. 6), supporting the igneous interpretation of the high-amplitude reflections in the Hel Graben. A major sill complex below thin basalts is similarly imaged on electromagnetic data on the Vøring Marginal High (Fig. 14).

### 3.3 Satellite Images and Topography

Satellite images and topographic data can be used to identify erosional resistant igneous intrusions. The mafic intrusions have different mechanical and chemical properties than the intruded host rocks, and sills and dykes form characteristic erosional highs in arid and Arctic environments (Fig. 3a). Google Earth images from the Karoo Basin, South Africa, and the Sverdrup Basin, Arctic Canada, reveal numerous well-defined saucer-shaped sill intrusions (Fig. 15). The mafic nature of these outcrops is confirmed by field studies (e.g., Polteau et al. 2008; Evenchick and Embry 2012).

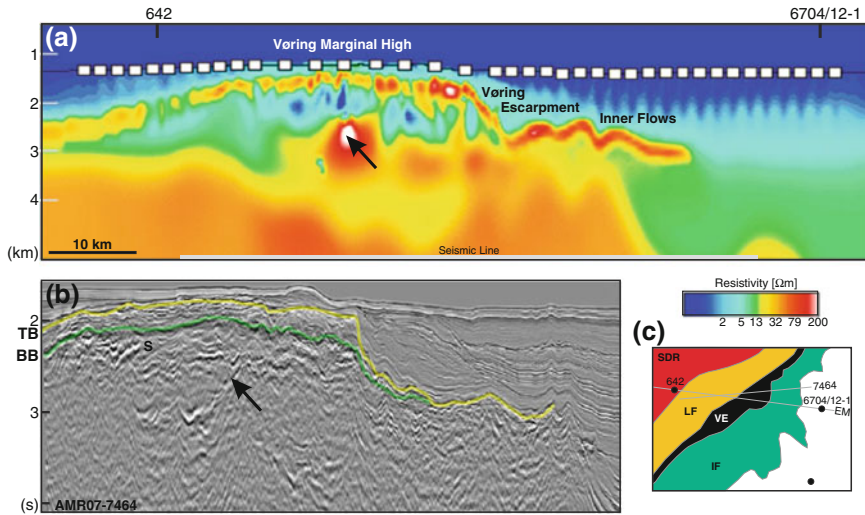


**Fig. 14** a Resistivity structure of a 2D profile across the outer Vøring Basin derived from CSEM inversion by EMGS. A thin, ca. 0.5 km, basalt sequence is identified as a high resistivity unit at 1.5–3.0 km depth. Low resistivities below this unit suggest the presence of kilometre thick sub-basalt sedimentary sequences. This interpretation is corroborated by interpretation of nearby seismic

profiles (b *TB* top basalt, *BB* base basalt, *S* sill). A very high resistive unit in the middle of the profile (*black arrow*) corresponds to a high-amplitude saucer-shaped reflection interpreted as a major sill. The map, c, shows the location of the profiles, wells and volcanic seismic facies units (*IF* inner flows, *VE* Vøring escarpment, *LF* landward flows, *SDR* seaward dipping reflections)

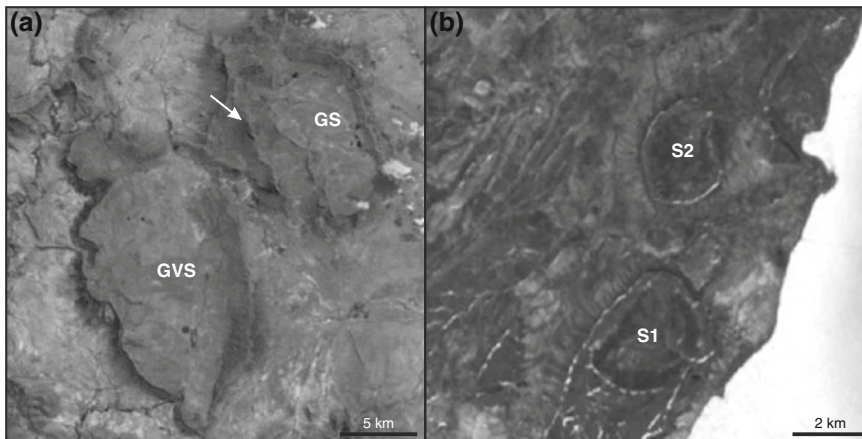


**Fig. 15** Modified Google Earth images of erosional remnants of saucer-shaped sills. a The Golden Valley Sill Complex (31.9S, 26.3E), Karoo Basin, South Africa. *GVS* Golden Valley Sill; *GS* Glen Sill. *Arrow* shows shallow-

level sills between *GVS* and *GS* possibly linking the intrusions. b Ellef Ringnes sill complex (79.0N, 102.8W), Sverdrup Basin, Canada. *S1*, *S2* Saucer-shaped sills

## 4 Summary

Igneous intrusions such as sills, dykes, and laccoliths are abundant in sedimentary basins, and are often associated with continental and volcanic rifted margin Large Igneous Provinces. Mafic igneous intrusions are characterized by high seismic velocities in the range from 5.0 to 7.0 km/s. Velocity aureoles with a thickness comparable to the sill intrusion are commonly identified on sonic log data above and below the intrusions. Sills as thin as 10 m may be detected by conventional seismic reflection data, whereas sills with a thickness above about 40 m are resolvable. Deeper sills are more difficult to image as the wave amplitudes decay across the uppermost sill due to transmission losses across the high-impedance boundaries at the top and the base of the sills. Offset-dependent tuning is expected for high-velocity sills due to the high-velocity of the intrusions. The velocity of intrusions in sill-sediment complexes can be derived from wide-angle ocean bottom seismometer data if the sills are sufficiently abundant.

Sill reflections are interpreted based on characteristic features such as high amplitude reflections with saucer-shaped geometries. Sill complexes are well-suited for 3D visualization techniques and abundant new information about sill geometries and emplacement dynamics have been obtained by such methods over the past decade. Potential field and electromagnetic data may improve sill interpretation; however such data have a poor resolution if sills are buried below more than a few kilometres of sediments. In contrast, field studies of volcanic basins such as the Karoo Basin in South Africa have provided a lot of complementary information about intrusive sill complexes. Dykes and laccoliths are less abundant than sills in volcanic basins, and few well-documented geophysical interpretation studies of such intrusions are published. Geophysical interpretation studies of andesitic and felsic intrusions are also rare.

**Acknowledgments** Special thanks to Audun Groth, Statoil, and VoxelVision for seismic visualization. Seismic data were kindly provided by TGS and EM data by

EMGS. This work was partly supported by the Research Council of Norway through its Centres of Excellence funding scheme, project number 223272.

## References

- Aarnes I, Svensen H, Connolly JAD, Podladchikov YP (2010) How contact metamorphism can trigger global climate changes: modeling gas generation around igneous sills in sedimentary basins. *Geochim Cosmochim Acta* 74:7179–7195
- Bell B, Butcher H (2002) On the emplacement of sill complexes: evidence from the Faroe-Shetland basin. *Geol Soc, London, Spec Publ* 197:307–329
- Berndt C, Skogly O, Planke S et al (2000) High-velocity breakup-related sills in the Vøring Basin, off Norway. *J Geophys Res: Solid Earth* 105:28443–28454
- Bryan SE, Ernst RE (2008) Revised definition of large igneous provinces (LIPs). *Earth Sci Rev* 86:175–202
- Bryan SE, Ferrari L (2013) Large igneous provinces and silicic large igneous provinces: progress in our understanding over the last 25 years. *Geol Soc Am Bull* 125:1053–1078. doi:10.1130/B30820.1
- Cartwright J, Hansen DM (2006) Magma transport through the crust via interconnected sill complexes. *Geology* 34:929–932
- Chevallier L, Woodford A (1999) Morpho-tectonics and mechanism of emplacement of the dolerite rings and sills of the western Karoo, South Africa. *S Afr J Geol* 102:43–54
- Evenchick CA, Embry AF (2012) *Geology, Ellef Rignes Island north Nunavut: Map 86 (preliminary)*. In: Canadian geoscience. Geological Survey of Canada
- Favretto-Cristin N, Cristini P, Bazelaire E (2009) What is a seismic reflector like? *Geophysics* 74:T13–T23
- Gernigon L, Ringenbach JC, Planke S, Le Gall B, Jonquet-Kolstø H (2003) Extension, crustal structure and magmatism at the outer Vøring Basin, Norwegian margin. *J Geol Soc London* 160:197–208
- Gernigon L, Ringenbach JC, Planke S, Le Gall B (2004) Deep structures and breakup along volcanic rifted margins: insights from integrated studies along the outer Vøring Basin (Norway). *Mar Pet Geol* 21:363–372
- Gibb F, Kanaris-Sotiriou R (1988) The geochemistry and origin of the Faeroe-Shetland sill complex. *Geol Soc, London, Spec Publ* 39:241–252
- Hansen DM, Cartwright J (2006a) Saucer-shaped sill with lobate morphology revealed by 3D seismic data: implications for resolving a shallow-level sill emplacement mechanism. *J Geol Soc* 163:509–523
- Hansen DM, Cartwright J (2006b) The three-dimensional geometry and growth of forced folds above saucer-shaped igneous sills. *J Struct Geol* 28:1520–1535
- Hansen DM, Cartwright JA, Thomas D (2004) 3D seismic analysis of the geometry of igneous sills and sill junction relationships. *Geol Soc, London, Memoirs* 29:199–208

- Holford SP, Schofield N, Macdonald JD et al (2012) Seismic analysis of igneous systems in sedimentary basins and their impacts on hydrocarbon prospectivity: examples from the southern Australian margin. *APPEA J* 52:229–252
- Magee C, Jackson CA-L, Schofield N (2013) The influence of normal fault geometry on igneous sill emplacement and morphology. *Geology* 41:407–410
- Miles A, Cartwright J (2010) Hybrid flow sills: a new mode of igneous sheet intrusion. *Geology* 38:343–346
- Neumann ER, Svensen H, Tegner C et al (2013) Sill and lava geochemistry of the mid-Norway and NE Greenland conjugate margins. *Geochem Geophys Geosyst* 14:3666–3690
- Pant DR, Greenhalgh SA (1989) Lateral resolution in seismic reflection—a physical model study. *Geophys J* 97:187–198
- Planke S, Cambray H (1998) Seismic properties of flood basalts from hole 917A downhole data, Southeast Greenland Volcanic Margin. *Proc ODP Sci Results* 152:453–462
- Planke S, Myklebust R (1999) Når seismikken kommer til kort. *GEO, Trondheim* 10:20–22
- Planke S, Rasmussen T, Rey S et al (2005) Seismic characteristics and distribution of volcanic intrusions and hydrothermal vent complexes in the Vøring and Møre basins. In: Geological Society, London, petroleum geology conference series. Geological Society of London, pp 833–844
- Polteau S, Mazzini A, Galland O et al (2008) Saucer-shaped intrusions: occurrences, emplacement and implications. *Earth Planet Sci Lett* 266:195–204
- Puryear CI, Castagna JP (2008) Layer-thickness determination and stratigraphic interpretation using spectral inversion. *Geophysics* 73:R37–R48
- Rocchi S, Mazzotti A, Marroni M et al (2007) Detection of Miocene saucer-shaped sills (offshore Senegal) via integrated interpretation of seismic, magnetic and gravity data. *Terra Nova* 19:232–239
- Rodriguez Monreal F, Villar HJ, Baudino R, Delpino D, Zencich S (2009) Modeling an atypical petroleum system: a case study of hydrocarbon generation, migration and accumulation related to igneous intrusions in the Neuquén Basin, Argentina. *Mar Pet Geol* 26:590–605
- Schofield A, Totterdell JM (2008) Distribution, timing and origin of magmatism in the Bight and Eucla basins. In: *Geoscience Australia*, p 19
- Schofield NJ, Brown DJ, Magee C et al (2012) Sill morphology and comparison of brittle and non-brittle emplacement mechanisms. *J Geol Soc* 169:127–141
- Skogseid J, Eldholm O (1989) Vøring Plateau continental margin: seismic interpretation, stratigraphy and vertical movements. *Proc Ocean Drill Program Sci Results* 104:993–1030
- Skogseid J, Pedersen T, Eldholm O et al (1992) Tectonism and magmatism during NE Atlantic continental break-up: the Vøring Margin. *Geol Soc, London, Spec Publ* 68:305–320
- Skogly OP (1998) Seismic characterization and emplacement of intrusives in the Vøring Basin. Cand Scient thesis, Department of Geology, University of Oslo
- Smallwood J, Harding A (2009) New seismic imaging methods, dating, intrusion style and effects of sills: a drilled example from the Faroe-Shetland basin. In: Varming T, Ziska H (eds) Second Faroe Islands exploration conference. Sindri–Jardfeingi, Torshavn, Faroe Islands, pp 104–123
- Svensen H, Planke S, Malthe-Sørenssen A et al (2004) Release of methane from a volcanic basin as a mechanism for initial Eocene global warming. *Nature* 429:542–545
- Svensen H, Planke S, Corfu F (2010) Zircon dating ties NE Atlantic sill emplacement to initial Eocene global warming. *J Geol Soc* 167:433–436
- Thomson K (2004) Sill complex geometry and internal architecture: a 3D seismic perspective. *Physical geology of high-level magmatic systems*. Geol Soc, London, Spec Publ 234:229–232
- Thomson K (2007) Determining magma flow in sills, dykes and laccoliths and their implications for sill emplacement mechanisms. *Bull Volc* 70:183–201
- Thomson K, Schofield N (2008) Lithological and structural controls on the emplacement and morphology of sills in sedimentary basins. *Geol Soc, London, Spec Publ* 302:31–44
- Trude K (2004) Kinematic indicators for shallow level igneous intrusions from 3D seismic data: evidence of flow direction and feeder location. *Geol Soc, London, Memoirs* 29:209–218
- Trude J, Cartwright J, Davies RJ et al (2003) New technique for dating igneous sills. *Geology* 31:813–816
- Widess MB (1973) How thin is a thin bed. *Geophysics* 38:1176–1254
- White R, Smith L, Roberts A et al (2008) Lower-crustal intrusion on the North Atlantic continental margin. *Nature* 452:460–464
- Zhang R, Castagna J (2011) Seismic sparse-layer reflectivity inversion using basis pursuit decomposition. *Geophysics* 76:147–158